Soft Matter

ARTICLE TYPE

Cite this: DOI: 00.0000/xxxxxxxxxx

Dense shearing flows of soft, frictional cylinders

Diego Berzi,[a] Kevin E. Buettner,[b,c] and Jennifer S. Curtis[d]

Received Date
Accepted Date

DOI: 00.0000/xxxxxxxxxx

We perform discrete numerical simulations at constant volume of dense, steady, homogeneous flows of true cylinders interacting via Hertzian contacts, with and without friction, in the absence of preferential alignment. We determine the critical values of solid volume fraction and average number of contacts per particle above which rate-independent components of the stresses develop, along with a sharp increase in the fluctuations of angular velocity. We show that kinetic theory, extended to account for velocity correlation at solid volume fractions larger than 0.49, can quantitatively predict the measured fluctuations of translational velocity, at least for sufficiently rigid cylinders, for any values of the cylinder aspect ratio and friction here investigated. The measured pressure above and below the critical solid volume fraction is in agreement with a recent theory originally intended for spheres that conjugates extended kinetic theory, the finite duration of collisions between soft particles and the development of an elastic network of long-lasting contacts responsible for the rate-independency of the flows in the supercritical regime. Finally, we find that, for sufficiently rigid cylinders, the ratio of shear stress to pressure in the subcritical regime is a linear function of the ratio of the shear rate to a suitable measure of the fluctuations of translational velocity, in qualitative accordance with kinetic theory, with an intercept that increases with friction. A decrease in the particle stiffness gives rise to nonlinear effects that greatly diminishes the stress ratio.

1 Introduction

Granular flows composed of non-spherical particles are encountered in a number of applications, ranging from industry to geophysics. Reliable mathematical models of flows of particles with complicated shape would permit, e.g., to increase the efficiency and decrease the energy required for handling and transporting granular materials in industrial apparati.

Discrete modelling of granular flows composed of spheres have been around for a long time[1] and are now able to deal with a number of complicated effects such as aggregation, breakage, cohesion and poly-dispersity.[2–5] Continuum models that extend the seminal works on kinetic theory of granular gases[6,7] to account for strong inelasticity,[8] friction,[9–11] velocity correlation,[12,13] finite stiffness and presence of rate-independent components of the stresses[14] can now satisfactorily reproduce the flows of rigid and soft spheres in a number of geometrical configurations.

In the last decade, discrete element simulations of shearing flows of true cylinders[15–18] and spherocylinders[19–22] have also been carried out. These simulations confirmed the experimental observation[23,24] that non-spherical particles, in which the ratio of major-to-minor axis is sufficiently far from one, develop a preferential alignment. This has a number of consequences on the constitutive relations to be adopted in continuum models.[19,21,25–28] In particular, it means that at least the mean orientation angle should be treated as an additional state variable, while phrasing the associated evolution equation.[29]

Kinetic theory of granular gases is capable of predicting stresses and velocity fluctuations in homogeneous shearing flows of frictionless cylinders in a wide range of length-to-diameter (aspect) ratio and solid volume fraction.[30,31] To do that, one has to introduce a number of phenomenological, although physically sound, modifications: the critical solid volume fraction at which the functions of kinetic theory diverge, because the particles are on average in close contact, depends on the cylinder aspect ratio;[30] the shape of the particles induces rotation in collisions even in the absence of friction, so that the effective coefficient of restitution (the negative ratio of post- to pre-collisional normal relative velocity between two impending cylinders) in the rate of collisional dissipation of fluctuation kinetic energy is less than the actual value set in the numerical simulations;[31] a measure of the cylinder alignment, relevant when the aspect ratio is less than 0.5 or greater than 2, must be taken into account in the expressions of the shear stress[30] and was shown to increase the correlation in the particle velocity fluctuations at solid volume fractions larger than 0.49.[31]

Here, we extend our previous works to include the roles of friction and stiffness on the steady, homogeneous, shearing flows

[a] Politecnico di Milano, 20133 Milano, Italy. E-mail: diego.berzi@polimi.it
[b] University of Florida, 32611 Gainesville, FL, USA.
[c] ExxonMobil Research and Engineering, 77389 Spring, TX, USA.
[d] University of California, 95616 Davis, CA, USA.

of cylinders. We perform discrete numerical simulations of true cylinders, interacting through inelastic, Hertzian contacts, in the absence of preferential alignment, at solid volume fractions as large as 0.68 and measure stresses, average number of contacts per particle, translational and rotational velocity fluctuations. This permits us to first identify the dependence of the critical volume fraction, at which the cylinders are on average in close contact, on particle friction and aspect ratio. We then highlight similarities and differences with what is observed in the case of soft, frictional spheres in terms of velocity fluctuations and stresses. We also show that the stresses can be qualitatively, and sometimes even quantitatively, predicted by constitutive relations that merge contributions associated with collisional exchange of momentum, modelled with extended kinetic theory, and elastic deformations of the contact network, once the critical volume fraction is exceeded.

2 Simulations

True, identical cylinders of mass density ρ_p, diameter d and length l are placed in a cell of constant volume and subjected to steady, homogeneous shearing in the absence of gravity. The flow, gradient and vorticity directions are x, y and z, respectively (Fig. 1).

Periodic, in the x- and z-directions, and Lees-Edwards,[32] in the y–direction, boundary conditions ensure that, once the simulation reaches a steady state, the x–component of the mean velocity, u, the only one present, is a linear function of y (that is, the shear rate u' is constant) and the flow is uniform. The number of cylinders in the cell is chosen to attain the desired solid volume fraction ν, in the range between 0.5 and 0.68.

Cylinders interact via Hertzian contact model in the normal direction, with Young's modulus E and a fixed Poisson ratio ψ equal to 0.3; and Coulomb sliding in the tangential direction, with μ the coefficient of sliding friction. The normal contact is damped to mimic the energy dissipation due to the propagation of elastic waves inside the material; this results in a coefficient of normal restitution e_n that we kept constant and equal to 0.95. More details about the numerical implementation of the discrete simulations are reported elsewhere.[15–17]

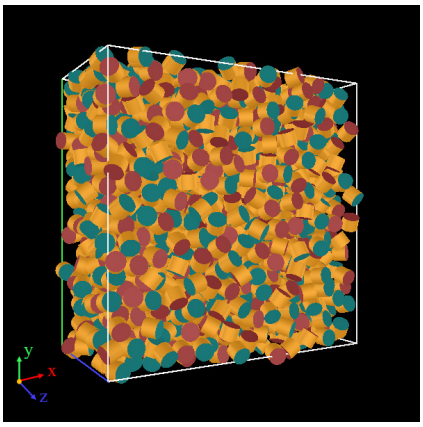

Fig. 1 Snapshot of a simulated dense shear flow of cylinders with aspect ratio $l/d = 0.8$.

We vary the aspect ratio l/d, from 0.5 to 2, the surface friction μ, from 0 to 1, and the dimensionless Young's modulus $E/\left(\rho_p u'^2 d_v^2\right)$ (where d_v is the equivalent diameter of a sphere having the same volume of the cylinder), from $2.6 \cdot 10^4$ to $2.6 \cdot 10^8$, and report in the following section measurement of coordination number Z (average number of contacts per particle), average rotational and translational velocity fluctuations, particle pressure p and shear stress s. In all simulations, the order parameter, that is the largest eigenvalue of a symmetric traceless tensor measuring the average orientation of the cylinders,[23] is always less than 0.35, well below the value 0.6 above which a phase transition between a disordered, gaseous and a liquid crystal state takes place in the frictionless case.[30,31]

3 Results and modelling

3.1 Critical point

Discrete element simulations of steady, homogeneous shearing flows of soft, identical spheres at constant volume[33,34] show that, above a critical value ν_c of the solid volume fraction that is only a function of the sliding friction μ, the stresses are characterized by rate-independent components proportional to the particle stiffness. In the proximity of ν_c, average stresses and translational velocity fluctuations dramatically increase[11] while fluctuations in pressure and coordination number peak.[34]

Peaks in the fluctuations of Z have also permitted to identify ν_c in the case of steady, *inhomogeneous* shearing flows[35,36] and confirm the presence of rate-independent components of the stresses above the critical solid volume fraction. Rate-independency has instead been observed at values of the coordination number larger than a critical Z_c in the case of *unsteady*, homogeneous shearing flows[37] at constant volume fractions less than ν_c. Depending on the flow configuration, then, either ν_c or Z_c can determine the phase transition from a purely rate-dependent to a combination of rate-dependent and rate-independent stresses.

Actually, in steady, homogeneous shearing, there is a one-to-one relation between solid volume fraction and coordination number, so that when $\nu = \nu_c$ also $Z = Z_c$. It has been suggested[14] that at solid volume fractions larger than ν_c the spheres in the discrete simulations are on average overlapped, thus creating a continuously rearranging network of slightly compressed springs. This would explain why the rate-independent components of the stresses are proportional to the particle stiffness. It also implies that, at the critical solid volume fraction, the average overlap between the spheres as well as the average interparticle distance, at least along the principal axis of compression, are exactly zero. Instead, the average interparticle distance measured along the principal axis of extension might be nonzero. This anisotropy, associated also with differences in the normal stresses,[38,39] increases with friction,[33] hence providing a physical explanation of the monotonic decrease of ν_c (and Z_c) with μ.

If the average overlap is zero at ν_c, then the particle stiffness should play little to no role there. In the plane ν–Z, curves obtained on steady, homogeneous shearing flows of spheres of different dimensionless particle stiffness are expected to intersect at the critical point ν_c–Z_c. This was indeed firstly observed many

years ago[40] and exploited to determine the critical values of solid volume fraction and coordination number for frictionless[41] and frictional[42] spheres.

Our discrete numerical simulations reveal that curves of coordination number against solid volume fraction, measured for values of the dimensionless Young's modulus that differ in orders of magnitude, also intersect at a critical point in the case of steady, homogeneous shearing flows of true cylinders (an example is reported in Fig. 2a). This permits us to obtain the dependence of ν_c and Z_c on the friction coefficient μ for different cylinder aspect ratios and make comparisons with previous results on spheres (Figs. 2b and c). Both ν_c and Z_c monotonically decrease with μ irrespective of the particle geometry, hinting at the crucial role that friction plays on the spatial anisotropy in the particle arrangement also in the case of cylinders. The critical coordination number is always less for spheres than for cylinders (Fig. 2c). On the other hand, the critical solid volume fraction is less for frictionless spheres than for frictionless cylinders, whereas the opposite is true when friction exceeds 0.3 (Fig. 2b).

3.2 Velocity fluctuations

If we define as C and Ω the fluctuation in translational and angular velocity, respectively, with respect to their average values, we can measure the intensities of such fluctuations in the simulations via the translational temperature, $T = \langle C^2 \rangle /3$, and the rotational temperature, $\Theta = I \langle \Omega^2 \rangle / N_{rot} m$,[43] where the angular brackets denote ensemble averaging and N_{rot} is the number of rotational degrees of freedom (2 or 3 for frictionless or frictional cylinders, respectively). In the expression of Θ, I is the moment of inertia and m is the mass of the particle. In steady, homogeneous granular flows, the ratio Θ/T is a measure of how much translational fluctuation energy is transformed into rotational fluctuation energy.[44] As such, it is an indicator of the geometry of the collisions at the microscopic level.[45]

Figure 3a depicts the behaviour of the measured ratio Θ/T as a function of $\nu - \nu_c$ –with the critical volume fraction given in Fig. 2b– in our simulations on cylinders with $E/\left(\rho_p u'^2 d_v^2\right) = 2.6 \cdot 10^8$ for all the investigated values of friction and aspect ratio. Also shown are the theoretical predictions in the case of spheres.[10]

Spheres and cylinders behave very differently. Frictionless spheres interact through central forces, i.e., directed along the line joining the centers of the particles, so that rotation cannot be induced in contacts, and therefore the rotational temperature is zero. Collisions between frictionless cylinders can instead generate rotation, and indeed the fluctuations in the angular velocity are about the same as the fluctuations in the translational velocity, irrespective of the cylinder aspect ratio and the solid volume fraction (Fig. 3a).

When μ increases, more and more spheres interact through rolling contacts and the ratio Θ/T increases. Unexpectedly, this is not the case for frictional cylinders. Apart from a few points, we observe a nice collapse, irrespective of aspect ratio and friction coefficient, as long as the latter is nonzero: Θ/T is roughly constant and about 0.4 at solid volume fractions less than the critical and dramatically increases for $\nu > \nu_c$ (Fig. 3a). The increasing

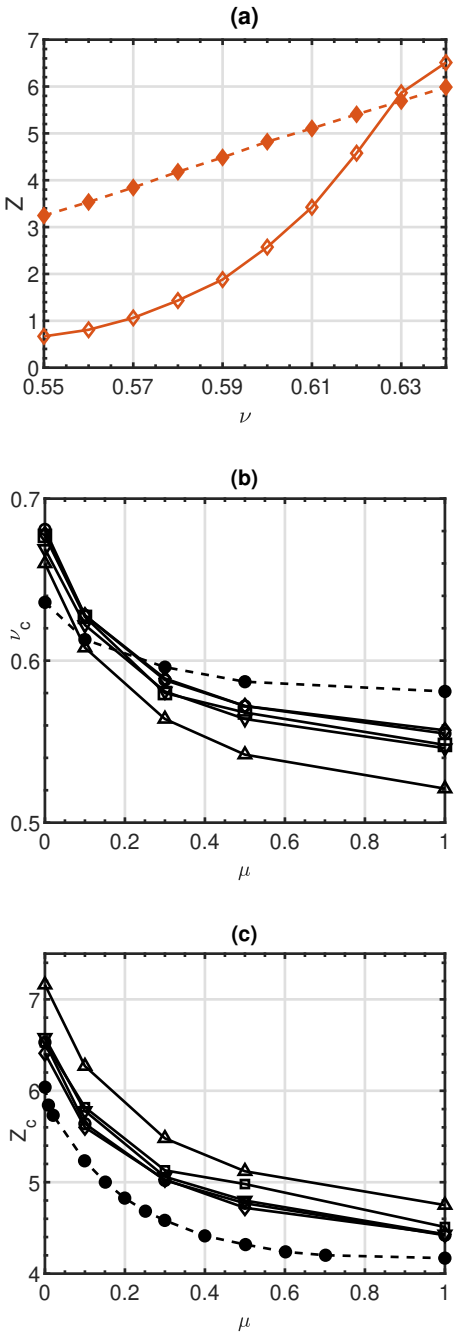

Fig. 2 (a) Measured coordination number against solid volume fraction for cylinders with aspect ratio $l/d = 0.8$, sliding friction $\mu = 0.1$, and Young's modulus $E/\left(\rho_p u'^2 d_v^2\right) = 2.6 \cdot 10^8$ (hollow diamonds) and $E/\left(\rho_p u'^2 d_v^2\right) = 2.6 \cdot 10^4$ (solid diamonds). Critical (b) solid volume fraction and (c) coordination number as functions of sliding friction for spheres (solid circles, after[33]) and cylinders with aspect ratio l/d equal to: 0.5 (squares); 0.8 (diamonds); 1 (hollow circles); 1.25 (lower triangles); 2 (upper triangles).

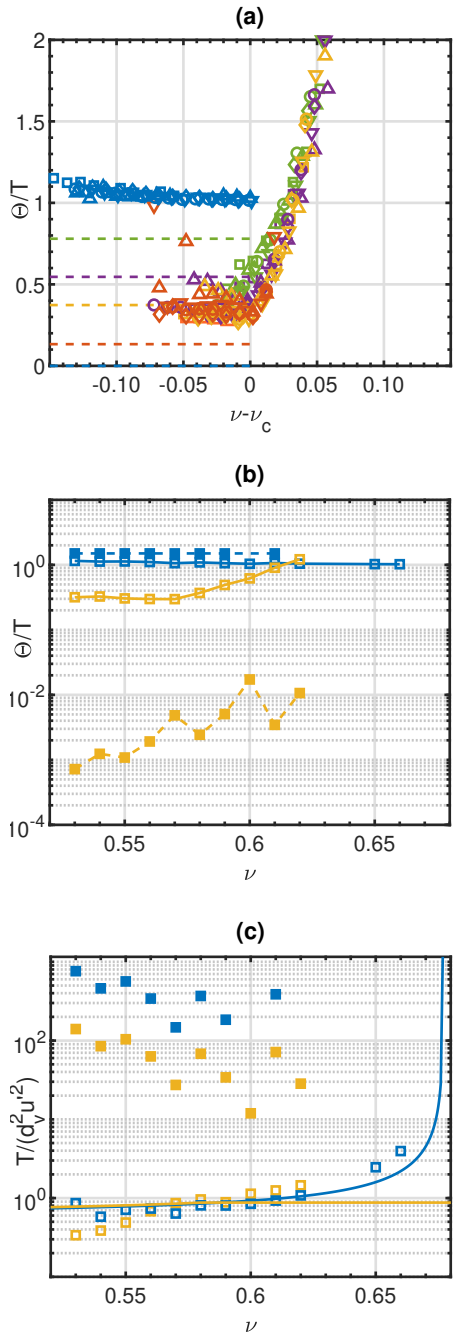

Fig. 3 (a) Measured ratio of rotational to translational temperature against the deviation from the critical solid volume fraction for cylinders with different aspect ratios (same symbols as in Fig. 2) and $E/\left(\rho_p u'^2 d_v^2\right) = 2.6\cdot 10^8$ when: $\mu = 0$ (blue symbols); $\mu = 0.1$ (orange symbols); $\mu = 0.3$ (yellow symbols); $\mu = 0.5$ (purple symbols); $\mu = 1$ (green symbols). The dashed lines represent the theoretical predictions in the case of spheres. Measured (b) ratio of rotational to translational temperature and (c) dimensionless translational temperature against the solid volume fraction for cylinders with $l/d = 0.5$, $\mu = 0$ (blue squares) and $\mu = 0.3$ (yellow squares), and $E/\left(\rho_p u'^2 d_v^2\right) = 2.6\cdot 10^8$ (hollow squares) and $E/\left(\rho_p u'^2 d_v^2\right) = 2.6\cdot 10^4$ (solid squares). The solid lines in Fig. 3c are the predictions of extended kinetic theory (Eqs. 1 and 2).

fluctuations in angular velocity with the distance from the critical point are further evidence that a phase transition takes place there.

Decreasing the particle stiffness by 4 orders of magnitude slightly increases the ratio Θ/T in the case of frictionless cylinders. In the case of frictional cylinders, instead, Θ/T decreases by 2 to 3 orders of magnitude (see an example in Fig. 3b for $l/d = 0.5$; we obtained similar results, not shown here for brevity, for all aspect ratios).

Decreasing the cylinder stiffness greatly increases the fluctuations in translational velocity for both frictionless and frictional cylinders (Fig. 3c). However, Fig. 3b reveals that softer frictionless cylinders also experience larger fluctuations in rotational velocity, that are instead suppressed when friction is present. It has been shown, on the other hand, that stiffness plays a little role on the fluctuations in translational velocity in the case of frictional spheres.[14]

Extended kinetic theory,[13,46] that is kinetic theory which takes into account the decrease in the collisional rate of dissipation of translational fluctuation energy due to correlation in velocities that develops once the freezing point, $\nu = 0.49$,[47] is exceeded, predicts the dependence of the dimensionless translational temperature on the solid volume fraction in dense, homgeneous shearing flows of spheres as[14]

$$\frac{T}{d_v^2 u'^2} = \frac{2J_\infty}{15\left(1-\varepsilon^2\right)}\left[\frac{26\left(1-\varepsilon\right)}{15}\frac{\nu-0.49}{\nu_{rcp}-\nu}+1\right], \qquad (1)$$

when $\nu \leq \nu_c$, and

$$\frac{T}{d_v^2 u'^2} = \frac{2J_\infty}{15\left(1-\varepsilon^2\right)}\left[\frac{26\left(1-\varepsilon\right)}{15}\frac{\nu_c-0.49}{\nu_{rcp}-\nu_c}+1\right], \qquad (2)$$

when $\nu > \nu_c$. Here, $J_\infty = (1+e_n)/2 + \pi(1+e_n)^2(3e_n-1)/\left[96-24\left(1-e_n\right)^2-20\left(1-e_n^2\right)\right]$, while ν_{rcp} is the random close packing, which, for spheres, is roughly equal to the critical solid volume fraction ν_c when $\mu = 0$.[11] Here, we assume that the same applies to cylinders.

In Eqs. 1 and 2, ε is an effective coefficient of restitution that is used in the expression for the collisional dissipation rate of kinetic theory to incorporate the exchange between rotational and translational kinetic energy in the translational fluctuation energy balance and avoid the necessity of introducing an additional balance equation for the rotational fluctuation energy. For cylinders, ε should be a function of both the aspect ratio and the friction coefficient. Here, we have determined ε from the translational temperature measured in our simulations via linear regression by approximating Eqs. 1 and 2 as first-order Taylor series around $\varepsilon = e$, where e is the effective coefficient of restitution in the case of frictionless cylinders.[31] The obtained deviation $\varepsilon - e$ as a function of the friction coefficient is reported in Fig. 4. Also shown are the results in the case of spheres (for which $e = e_n$) and a previously suggested analytical expression.[48]

Figure 4 indicates that the influence of the particle geometry on the effective coefficient of restitution in the presence of friction cannot be simply captured through its value e in the absence of friction. We also notice that ε for cylinders seems to peak for

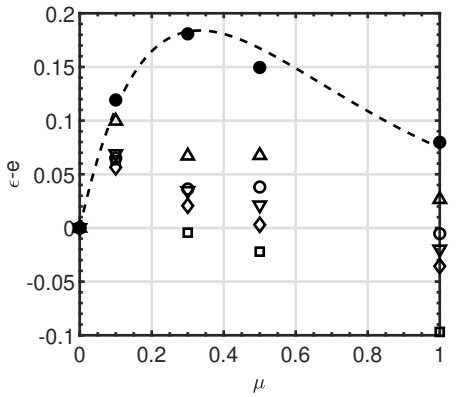

Fig. 4 Dependence of the deviation of the effective coefficient of restitution from its value at $\mu = 0$ on the friction coefficient for cylinders with different aspect ratios (same symbols as in Fig. 2a). Also shown are the results for spheres (solid circles) and the corresponding interpolating expression $\frac{3}{2}\mu\exp(-3\mu)$ (dashed line).[48]

μ about 0.1 (in the case of spheres the peak is closer to $\mu = 0.3$) and that the complicated interaction between friction and shape can even lead, counter-intuitively, to an effective coefficient of restitution that is higher for frictional than for frictionless cylinders. Finally, the collapse of Θ/T in the case of frictional cylinders (Fig. 3a) also points out that the effective coefficient of restitution is not simply a function of the temperature ratio, as in the case of spheres.[9,10]

When we employ the effective coefficient of restitution of Fig. 4 in Eqs. 1 and 2, we can satisfactorily reproduce the translational temperature measured in the simulations (see two examples in Fig. 3c; similar agreement is obtained for all values of friction and aspect ratio), at least for the stiffest particles. The translational temperature is, on the other hand, poorly predicted once the particle stiffness is reduced. A reduction of 4 orders of magnitude of the stiffness implies an increase in T of about 2 orders of magnitude, for both frictional and frictionless cylinders (Fig. 3c). The latter observation, and the difference between frictional and frictionless cylinders in terms of the relation between Θ/T and their stiffness (Fig. 3b), suggests that the increase in translational velocity fluctuations for softer cylinders has nothing to do with the role of fluctuations in the angular velocity. We instead suspect that the particle stiffness plays a role in determining the velocity correlation thus requiring larger fluctuations to dissipate the same amount of kinetic energy. We postpone this investigation to a future work.

3.3 Stresses

Kinetic theory of granular gases predicts that, for rigid spheres and, thus, instantaneous collisions, the pressure, p, is proportional to the translational temperature through a function of coefficient of normal restitution and volume fraction. In the case of soft spheres, at volume fraction less than the critical (subcritical regime), it was suggested[11] to account for the finite duration of contact, induced by the finite particle stiffness, by taking the dense limit of the expression of kinetic theory[8,46] and multiplying it by the ratio of the free flight time, t_f, to the sum of free flight time and contact duration, t_c:

$$p = \rho_p 2(1+e_n)\,\nu G T \frac{t_f}{t_f+t_c}, \tag{3}$$

where, in the neighborhood of the critical volume fraction, $G = 2\nu/(\nu_c-\nu)$[11,14]. In the case of Hertzian contacts:[11]

$$\frac{t_f}{t_f+t_c} = \left[1+30.5G\left(\rho_p T\frac{1-\psi^2}{E}\right)^{2/5}\right]^{-1}. \tag{4}$$

When the solid volume fraction of the spheres exceeds ν_c (supercritical regime), an elastic component of the pressure, proportional to the particle stiffness, is superimposed to a component still associated with collisional exchange of momentum, that is assumed to be expressed through Eq. 3, with, however, the denominator t_f+t_c replaced by t_c only (the time of free flight is taken to be zero when the interparticle distance is zero on average). In the case of Hertzian contacts, the supercritical pressure reads therefore:[11]

$$p = \rho_p 2(1+e_n)\,\nu G T\frac{t_f}{t_c} + \alpha_E\frac{E}{1-\psi^2}(\nu-\nu_c), \tag{5}$$

where α_E is a dimensionless numerical coefficient, and t_f/t_c is given by Eq. 4 where only the second term between square brackets is retained.

Using the definition of G and Eq. 4, we can recast the expression for the subcritical pressure (Eq. 3) as:

$$\left[\frac{p(1-\psi^2)}{E|\nu_c-\nu|}\right]^{-1} = \frac{1}{4(1+e_n)\,\nu^2}\left\{\left[\frac{\rho_p T(1-\psi^2)}{E(\nu_c-\nu)^2}\right]^{1/2}\right\}^{-2} + \frac{15.25}{(1+e_n)\,\nu(\nu_c-\nu)^{1/5}}\left\{\left[\frac{\rho_p T(1-\psi^2)}{E(\nu_c-\nu)^2}\right]^{1/2}\right\}^{-6/5}. \tag{6}$$

Similarly, the expression of the supercritical pressure (Eq. 5) can be re-written as:

$$\frac{p(1-\psi^2)}{E|\nu_c-\nu|} = \frac{(1+e_n)\,\nu(\nu_c-\nu)^{1/5}}{15.25}\left\{\left[\frac{\rho_p T(1-\psi^2)}{E(\nu_c-\nu)^2}\right]^{1/2}\right\}^{6/5} + \alpha_E. \tag{7}$$

If the analysis performed for spheres held also in the case of cylinders, Eqs. 6 and 7 would imply a collapse of the measured scaled pressure $p(1-\psi^2)/E/|\nu_c-\nu|$ as a function of the square root of the scaled translational temperature $\rho_p T(1-\psi^2)/E/(\nu-\nu_c)^2$, given the low variability of ν. Figure 5 indeed shows such a collapse, independent of the cylinder aspect ratio, friction and stiffness.

Similar collapses, with the scaled shear rate instead of the square root of T on the x-axis, have been previously obtained in the case of steady, homogeneous[34] and steady, inhomogeneous[35] flows of soft spheres. For unsteady, homogeneous flows of spheres, instead, the collapse can be obtained using the coordination number rather than the volume fraction in the scaling of

p and T.[42]

For the scaled T that tends to 0 (that is, for rigid particles or very low agitated soft particles), the plot of Fig. 5 shows two limiting behaviours. At volume fractions less than the critical, collisions are essentially binary and instantaneous, and the soft contribution to the subcritical pressure of Eq. 6 (the second term on the right hand side) is negligible. The scaled pressure is, therefore, proportional to the second power of the scaled square root of the temperature (rigid collisional limit[35] or inertial regime[34]).

For volume fractions larger than the critical, the elastic component of the supercritical pressure dominates in Eq. 7 and p is independent of T. The momentum exchange in collisions is negligible and an anisotropic contact network spans the entire domain, corresponding to a shear jammed condition,[35] also called the quasistatic regime.[34]

When the scaled T tends to infinity, Eqs. 6 and 7 coincide, and the pressure mainly arises because of momentum exchange in collisions, with the frequency of interaction set by the inverse of t_c. This has been termed the soft collisional limit[35] or intermediate regime.[34]

Equations 6 and 7 can reproduce the results of the numerical simulations (Fig. 5). There, for simplicity, we have taken $\nu = 0.6$ and $|\nu - \nu_c| = 0.05$, but the results are only mildly dependent on the solid volume fraction and the distance from its critical value, at least in the range investigated in the present work.

Part of the scattering of the data in Fig. 5 might be due to the residual dependence of the scaled pressure on the solid volume fraction, and on some role played by the aspect ratio. Also, we could have certainly improved the agreement between the measurements and the theory in the shear jammed limit, if we had taken different values of α_E as a function of friction (as done in[34] for spheres); and in the rigid collisional limit, if we had modified the numerical constant in the expression for G (a value larger than 2 for the case of frictionless cylinders and less than 2 for frictional cylinders). We claim, however, that these are simply details, while Eqs. 6 and 7 seem to capture the essential physics.

In the case of steady, homegeneous flows of soft spheres,[14] the dense limit expression of kinetic theory for the shear stress, s, reads[46]

$$\frac{s}{p} = \frac{4J_\infty}{5\pi^{1/2}(1+e_n)}\frac{d_v u'}{T^{1/2}}, \tag{8}$$

that is, the stress ratio s/p should be a linear function of the square root of the inverse dimensionless translational temperature through a function of the normal coefficient of restitution only, independently of friction (with $e_n = 0.95$, as in the present simulations, the coefficient of proportionality is about 0.28). Equation 8 also implies that, when the shear rate vanishes (yielding condition), the stress ratio vanishes as well.

Figure 6 indicates that Eq. 8 can indeed reproduce with sufficient accuracy the stress ratio measured in previous discrete simulations of steady, homogeneous shearing of spheres interacting via Hookean contacts[41,48], for different values of friction and coefficient of normal restitution, at $\nu < \nu_c$. These simulations were performed with dimensionless Young's moduli ranging from 10^3 to 10^7, and we notice that the lowest values of the stress ratio, corresponding to the largest values of the dimensionless T, are obtained with the stiffest particles.

Figure 7 depicts the measured dependence of the stress ratio on the square root of the inverse dimensionless T in the case of true cylinders, when $\nu \leq \nu_c$ (subcritical regime). For $d_v u'/T^{1/2} > 0.3$ (which roughly corresponds to the stiffest cylinders, with $E/\left(\rho_p u'^2 d_v^2\right) = 2.6 \cdot 10^8$), the data indeed confirm that s/p is proportional to $d_v u'/T^{1/2}$, with a coefficient of proportionality equal to 0.1, lower than the value 0.28 valid for spheres, independent of friction. However, unlike what is predicted by kinetic theory, the linear interpolation gives a nonzero intercept μ_s for $d_v u'/T^{1/2} = 0$, which increases with friction (see the caption of Fig.7). The estimated values of μ_s, that can be interpreted as the stress ratio at yielding, are similar to what was observed in the case of frictional, elongated sphero-cylinders.[21] At the lowest values of $d_v u'/T^{1/2}$, which, unlike for spheres, correspond to the softest cylinders, the measured stress ratio exhibits a nonlinear behaviour and can be extremely low (even less than 0.01). We believe that this behaviour can be captured only by nonlinear kinetic theories.[38,39] Without any theoretical justification, the data of Fig. 7 can be tentatively fitted by modified logistic functions of the form:

$$\frac{s}{p} = \frac{0.1 d_v u'/T^{1/2} + \mu_s}{1 + \exp\left(5 - 30 d_v u'/T^{1/2}\right)}. \tag{9}$$

When ν is larger than the critical, Eq. 9 still agrees with the measurements when $E/\left(\rho_p u'^2 d_v^2\right) = 2.6 \cdot 10^4$. However, there is a larger scattering when the stiffness increases, an indication that the stress ratio must depend on some parameters other than simply the inverse square root of the dimensionless T. In the case of spheres, for instance, the stress ratio at $\nu > \nu_c$ strongly depends on the anisotropy of the fabric tensor.[33]

4 Conclusions

We have performed discrete numerical simulations of dense, steady, homogeneous shearing flows of frictionless and frictional cylinders ineteracting via Hertzian contacts at different values of solid volume fraction and particle stiffness. The cylinder aspect ratio ranged from 0.5 to 2, sufficiently close to unity to avoid ordering in the alignment of the cylinder axis.

As for spheres, we have identified a critical point in the solid volume fraction–coordination number plane that marks the transition from a purely rate-dependent to a mixed regime, in which rate-dependent and rate-independent components of the stresses coexist. This critical point depends on the particle aspect ratio and surface friction, but is independent of the particle stiffness.

We have measured fluctuations in angular and translational velocity and confirmed that, due to the nonspherical shape, fluctuations in angular velocity are present even in the case of frictionless particles. Also in contrast with spheres, the ratio of the rotational to the translational temperature seems a unique function of the distance from the critical point for frictional cylinders, with a strong increase in the supercritical regime. The rotational temperature is only slightly affected by the particle stiffness, while the translational temperature increases by 2 orders of magnitude if the stiffness is reduced of 4 orders of magnitude. This effect has no parallel in the case of spheres, and it might point to an

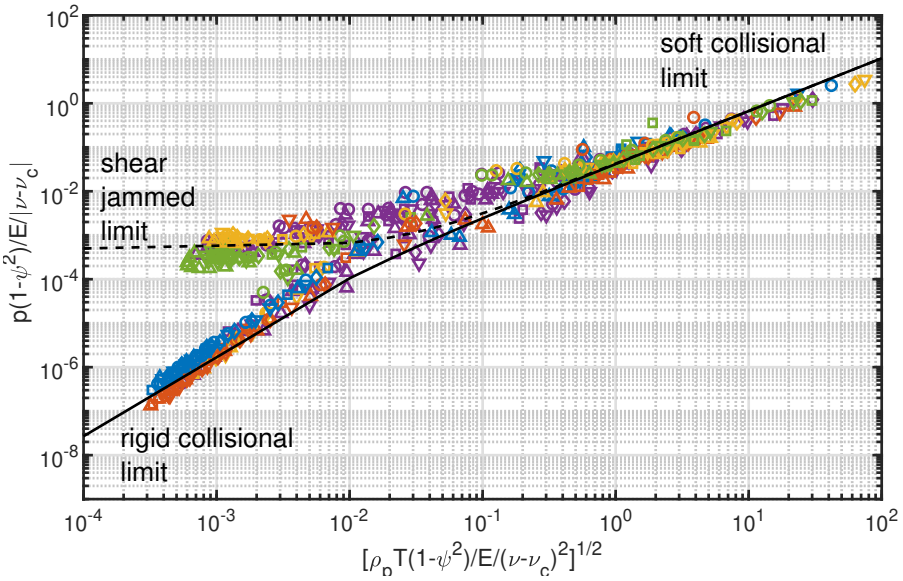

Fig. 5 Dependence of the scaled pressure on the square root of the scaled translational temperature in the case of true cylinders for all values of aspect ratio, friction and stiffness (same legend as in Fig. 3a). Also shown are the predictions of Eqs. 6 (solid line) and 7 (dashed line) when $\nu = 0.6$, $|\nu - \nu_c| = 0.05$ and $\alpha_E = 0.0005$.

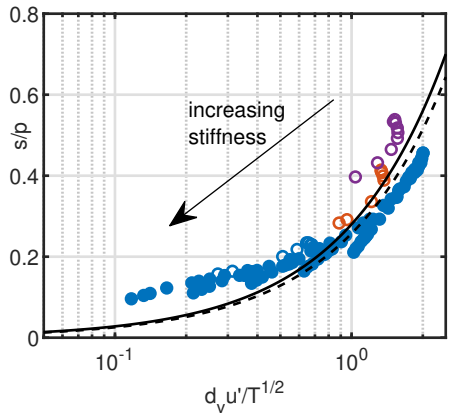

Fig. 6 Dependence of the subcritical stress ratio on the square root of the inverse dimensionless translational temperature in the case of spheres interacting via Hookean contacts, with $e_n = 0.95$ (hollow circles[48]) and $e_n = 0.7$ (solid circles[41]) and: $\mu = 0$ (blue symbols); $\mu = 0.1$ (orange symbols); $\mu = 0.5$ (purple symbols). Also shown are the predictions of Eq. 8 when $e_n = 0.95$ (solid line) and $e_n = 0.7$ (dashed line).

enhanced velocity correlation that decreases the rate at which translational, fluctuation kinetic energy is dissipated in collisions. For the stiffest cylinders, however, the dependence of the translational temperature on the solid volume fraction is well predicted using extended kinetic theory, once an appropriated effective coefficient of restitution depending on the particle aspect ratio and friction is adopted.

As in the case of spheres, the granular pressure exhibits three limits, corresponding to three physical regimes: (i) a rigid, collisional limit, at solid volume fractions less than the critical and large particle stiffness, in which particles exchange momentum in binary, instantaneous collisions; (ii) a shear jammed limit, at solid volume fractions larger than the critical and large particle stiffness, where a network of long lasting contacts spans the entire domain and stresses originate from the compression of the springs in the Hertzian contact model; (iii) a soft, collisional limit, in which particles exchange momentum in collisions at a frequency set by the inverse time scale associated with the spring compression. We have shown that a recent theory, developed for spheres, that incorporates the role of the particle stiffness in a kinetic theory and adds a component of the pressure proportional to the particle Young's modulus, can also describe the pressure in flows of true cylinders.

Finally, at solid volume fractions less than the critical, the ratio of shear stress to pressure is a linear increasing function of the inverse square root of the dimensionless translational temperature when the cylinders are sufficiently rigid. As in the case of elongated spherocylinders, measurements suggest the existence of a nonzero stress ratio in the limit of vanishing shear rate (yield) that increases with friction. Nonlinearity arises as the particle stiffness decreases, an effect that was never observed in the case of spheres. This nonlinear behaviour is particularly interesting be-

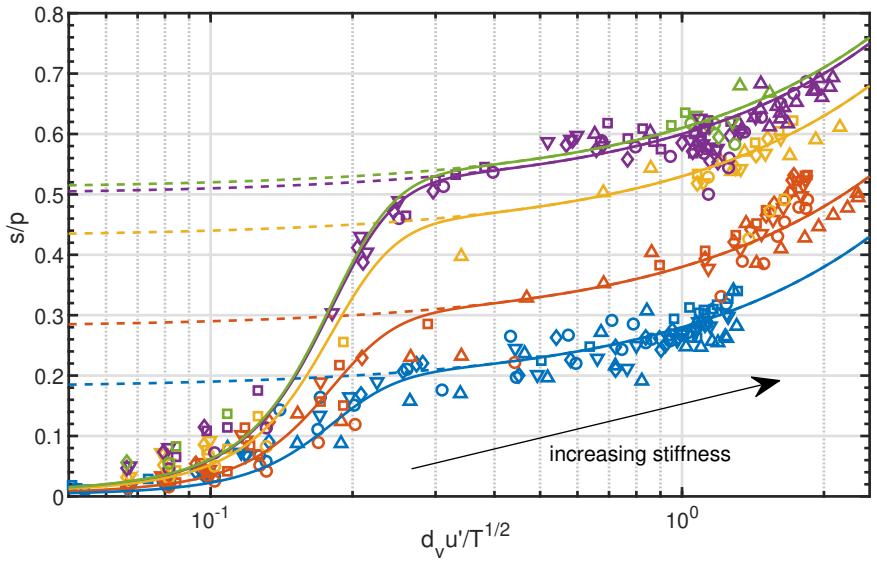

Fig. 7 Dependence of the subcritical stress ratio on the square root of the inverse dimensionless translational temperature in the case of true cylinders for all values of aspect ratio, friction and stiffness (same legend as in Fig. 3a). Also shown are the predictions of Eq. 9 (solid lines) and the associated linear asymptotes (dashed lines), with $\mu_s = 0.18$, 0.28, 0.43, 0.5, 0.51 when $\mu = 0$, 0.1, 0.3, 0.5, and 1, respectively.

cause it is associated with extremely low values of the stress ratio, sometimes termed as macroscopic friction, with possible practical applications.

Conflicts of interest

There are no conflicts to declare.

Acknowledgements

DB wishes to thank prof. James T. Jenkins for many stimulating discussions and invaluable suggestions. The authors also acknowledge the University of Florida Research Computing organization for providing computational resources and technical support.

Notes and references

1 P. A. Cundall and O. D. L. Strack, *Geotechnique*, 1979, **29**, 47–65.
2 S. Luding, *Granular Matter*, 2008, **10**, 235–246.
3 V. Ogarko and S. Luding, *Soft Matter*, 2013, **9**, 9530–9534.
4 N. Kumar, O. I. Imole, V. Magnanimo and S. Luding, *Particuology*, 2014, **12**, 64–79.
5 Y. Guo and J. S. Curtis, *Annual Review of Fluid Mechanics*, 2015, **47**, 21–46.
6 J. Jenkins and S. Savage, *Journal of Fluid Mechanics*, 1983, **130**, 187–202.
7 S. Savage and M. Sayed, *Journal of Fluid Mechanics*, 1984, **142**, 391–430.
8 V. Garzó and J. W. Dufty, *Physical Review E*, 1999, **59**, 5895–5911.
9 J. T. Jenkins and C. Zhang, *Physics of Fluids*, 2002, **14**, 1228–1235.
10 M. Larcher and J. T. Jenkins, *Physics of Fluids*, 2013, **25**, 113301.
11 D. Berzi and D. Vescovi, *Physics of Fluids (1994-present)*, 2015, **27**, 013302.
12 J. T. Jenkins, *Physics of Fluids*, 2006, **18**, 103307.
13 J. T. Jenkins, *Granular Matter*, 2007, **10**, 47–52.
14 D. Berzi and J. T. Jenkins, *Soft Matter*, 2015, **11**, 4799–4808.
15 M. Kodam, R. Bharadwaj, J. Curtis, B. Hancock and C. Wassgren, *Chemical Engineering Science*, 2010, **65**, 5852–5862.
16 Y. Guo, C. Wassgren, W. Ketterhagen, B. Hancock, B. James and J. Curtis, *Journal of Fluid Mechanics*, 2012, **713**, 1–26.
17 Y. Guo, C. Wassgren, W. Ketterhagen, B. Hancock and J. Curtis, *Powder Technology*, 2012, **228**, 193–198.
18 Y. Guo, C. Wassgren, B. Hancock, W. Ketterhagen and J. Curtis, *Physics of Fluids*, 2013, **25**, 063304.
19 D. B. Nagy, P. Claudin, T. Börzsönyi and E. Somfai, *Physical Review E*, 2017, **96**, 2–6.
20 T. Marschall, Y. E. Keta, P. Olsson and S. Teitel, *Physical Review Letters*, 2019, **122**, 188002.
21 D. B. Nagy, P. Claudin, T. Börzsönyi and E. Somfai, *New Journal of Physics*, 2020, **22**, 073008.
22 T. A. Marschall and S. Teitel, *Physical Review E*, 2020, **101**, 32907.
23 T. Börzsönyi, B. Szabó, G. Törös, S. Wegner, J. Török, E. Somfai, T. Bien and R. Stannarius, *Physical Review Letters*, 2012, **108**, 228302.
24 T. Börzsönyi, B. Szabó, S. Wegner, K. Harth, J. Török, E. Somfai, T. Bien and R. Stannarius, *Physical Review E - Statistical, Nonlinear, and Soft Matter Physics*, 2012, **86**, 1–8.
25 X. Hong, M. Kohne, M. Morrell, H. Wang and E. R. Weeks, *Physical Review E*, 2017, **96**, 1–9.

26 A. Ashour, T. Trittel, T. Börzsönyi and R. Stannarius, *Physical Review Fluids*, 2017, **2**, 1–9.

27 R. Stannarius, D. Sancho Martinez, T. Finger, E. Somfai and T. Börzsönyi, *Granular Matter*, 2019, **21**, 1–10.

28 K. Harth, J. Wang, T. Börzsönyi and R. Stannarius, *Soft Matter*, 2020, **16**, 8013–8023.

29 B. Nadler, F. Guillard and I. Einav, *Physical Review Letters*, 2018, **120**, 198003.

30 D. Berzi, N. Thai-Quang, Y. Guo and J. Curtis, *Physical Review E*, 2016, **93**, 040901.

31 D. Berzi, N. Thai-Quang, Y. Guo and J. Curtis, *Physical Review E*, 2017, **95**, 050901.

32 W. Lee, R. Bennett and K. Meagher, *A method of estimating magnitude of local earthquakes from signal duration*, U.s. geological survey technical report, 1972.

33 J. Sun and S. Sundaresan, *Journal of Fluid Mechanics*, 2011, **682**, 590–616.

34 S. Chialvo, J. Sun and S. Sundaresan, *Physical Review E*, 2012, **85**, 021305.

35 D. Berzi, J. T. Jenkins and P. Richard, *Soft Matter*, 2019, **15**, 7173–7178.

36 D. Berzi, J. T. Jenkins and P. Richard, *J. Fluid Mech*, 2020, **885**, A27.

37 D. Berzi and J. T. Jenkins, *Physical Review Fluids*, 2018, **3**, 094303.

38 S. Saha and M. Alam, *J. Fluid Mech*, 2016, **795**, 549–580.

39 J. T. Jenkins, M. Alam and D. Berzi, *Physical Review Fluids*, 2020, **5**, 072301(R).

40 S. Ji and H. H. Shen, *Journal of Rheology*, 2008, **52**, 87–103.

41 D. Vescovi and S. Luding, *Soft Matter*, 2016, **12**, 8616–8628.

42 D. Vescovi, D. Berzi and C. di Prisco, *Granular Matter*, 2018, **20**, 27.

43 K. E. Buettner, Y. Guo and J. S. Curtis, *Powder Technology*, 2020, **365**, 83–91.

44 C. Lun, *J. Fluid Mech*, 1991, **233**, 539–559.

45 O. Herbst, M. Huthmann and A. Zippelius, *Granular Matter*, 2000, **2**, 211–219.

46 J. T. Jenkins and D. Berzi, *Granular Matter*, 2010, **12**, 151–158.

47 S. Torquato, *Physical Review E*, 1995, **51**, 3170–3182.

48 S. Chialvo and S. Sundaresan, *Physics of Fluids*, 2013, **25**, 070603.